Chinese Journal of
POLYMER SCIENCE

ARTICLE

https://doi.org/10.1007/s10118-021-2609-9
Chinese J. Polym. Sci. **2021**, *39*, 1449–1458

Active Layer Morphology Engineering of All-polymer Solar Cells by Systematically Tuning Molecular Weights of Polymer Donors/Acceptors

Ning Wang[a,b], Ying-Jian Yu[a,b], Ru-Yan Zhao[a,b], Ji-Dong Zhang[a,b], Jun Liu[a,b*], and Li-Xiang Wang[a,b]

[a] *State Key Lboratory of Polymer Physics and Chemistry, Changchun Institute of Applied Chemistry, Chinese Academy of Sciences, Changchun 130022, China*
[b] *School of Applied Chemistry and Engineering, University of Science and Technology of China, Hefei 230026, China*

Electronic Supplementary Information

Abstract In all-polymer solar cells (APSCs), number-average molecular weights (M_ns) of polymer donors and polymer acceptors play an important role in active layer morphology and photovoltaic performance. In this work, based on a series of APSCs with power conversion efficiency of approaching 10%, we study the effect of M_ns of both polymer donor and polymer acceptor on active layer morphology and photovoltaic performance of APSCs. We select poly[4-(5-(4,8-bis(5-((2-butyloctyl)thio)thiophen-2-yl)-6-methylbenzo[1,2-*b*:4,5-*b*']dithiophen-2-yl)thiophen-2-yl)-5,6-difluoro-2-(2-hexyldecyl)-7-(5-methylthiophen-2-yl)-2*H*-benzo[*d*][1,2,3]triazole] (CD1) as the polymer donor and poly[4-(5-(5,10-bis(2-dodecylhexadecyl)-4,4,9,9-tetrafluuoro-7-methyl-4,5,9,10-tetrahydro3a,5,8,10-tetraaza-4,9-diborapyren-2-yl)thiophen-2-yl)-7-(5-methylthiophen-2-yl)benzo[*c*][1,2,5]thiadiazole] (PBN-14) as the polymer acceptor. The M_ns of polymer donor CD1 are 14.0, 35.5 and 56.1 kg/mol, respectively, and the M_ns of polymer acceptor PBN-14 are 32.7, 72.4 and 103.4 kg/mol, respectively. To get the desired biscontinueous fibrous network morphololgy of the polymer donor/polymer acceptor blends, at least one polymer should have high or medium M_n. Moreover, when the M_n of polymer acceptor is high, the active layer morphology and APSC device performance are insensitive to the M_n of polymer donor. The optimal APSC device performance is obtained when the M_n of both the polymer donor and the polymer acceptor are medium. These results provide a comprehensive and deep understanding on the interplay and the effect of M_n of polymer donors and polymer acceptors in high-performance APSCs.

Keywords All-polymer solar cells; Molecular weights; Polymer aggregation; Active layer morphology

Citation: Wang, N.; Yu, Y. J.; Zhao, R. Y.; Zhang, J. D.; Liu, J.; Wang, L. X. Active layer morphology engineering of all-polymer solar cells by systematically tuning molecular weights of polymer donors/acceptors. *Chinese J. Polym. Sci.* **2021**, *39*, 1449–1458.

INTRODUCTION

Polymer solar cells (PSCs) have received tremendous attention because of their great merits of solution processability with low cost, flexiblity and semi-transparency.[1−7] The mainstream PSCs use blends of polymer electron donor and small molecular electron acceptor as active layers. Another imporant kind of PSCs is all polymer solar cells (APSCs), which use blends of polymer electron donors and polymer electron acceptors as photoactive layers.[8−12] Compared with typical PSCs, APSCs have the great merits of excellent morphological stability and mechanical robustness.[21−25] Great efforts have been dovoted to the development of new polymer acceptors and optimization of polymer donor/polymer acceptors blend morphology.[26−31] As a result, in the past decade, power conversion efficiency (PCE) of APSCs has been dramatically enhanced and has reached the 15% milestone.[32−35] APSCs have emerged as a promising kind of photovoltaic technology.

Number-average molecular weight (M_n) of polymer materials plays an important role in active layer morphology and photovoltaic performance of PSCs. In typical PSCs employing polymer donor/small molecular acceptor blends, effects of M_n on active layer morphology and photovoltaic performance have been intensively studied.[36−38] In comparison, for APSCs, effects of M_n on polymer donor/polymer acceptor blend morphology are less understood. Morphology optimization of polymer donor/polymer acceptor blend is very different from that of polymer donor/small molecular acceptor blend. In the former case, polymer donor/polymer acceptor blend morphology optimization is always carried out by controlling the pre-aggregation tendency of polymer chains in solution.[39,40] This strategy has been successfully performed by changing the solvent, optimizing the solution temperature, dissolving the two polymers individually, *etc*.[41−43] Optimizing morphology of APSCs by controlling M_n of either polymer donors or polymer acceptors has been reported by several research

---

* Corresponding author, E-mail: liujun@ciac.ac.cn

Received April 20, 2021; Accepted May 17, 2021; Published online July 23, 2021

groups.[44–47] Increasing M_n leads to enhanced aggregation tendency of polymer chains in solution. However, its effects on active layer morpholgy and device performance of APSCs are different case by case. Moreover, as there are both polymer donors and polymer acceptors in active layer of APSCs, the interplay of M_ns of the two polymers is rarely studied. To date, only Marks *et al*. have optimized active layer morphology of APSCs by tuning M_ns of both polymer donor and polymer acceptor. Unfortunately, the APSC device performce is moderate, *i.e*. PCE<5%.[48,49] Therefore, it is important to study the interplay of M_n of both polymer donor and polymer acceptor on active layer morphology of high-performance APSCs.

In this study, we select a combination of polymer donor and polymer acceptor, which can achieve high PCE of 10% in APSCs. We systematically study the effect of M_n of the two polymers on active layer morphology and photovoltaic performance of APSCs and get several important conclusions. To obtain biscontinuous fibrous network morphology and give excellent APSC device performance, either the polymer donor or the polymer acceptor or both should have high M_n. When the M_n of the polymer acceptor is high, the APSC device performance is insensitive to the M_n of the other polymer. The optimal APSC device performance is obtained when the M_ns of both the polymer donor and the polymer acceptor are medium. This result provides a comprehensive understanding on the matching of M_n of polymer donors and polymer acceptors in high-performance APSCs.

EXPERIMENTAL

Materials

Poly[4-(5-(4,8-bis(5-((2-butyloctyl)thio)thiophen-2-yl)-6-methylbenzo[1,2-*b*:4,5-*b*']dithiophen-2-yl)thiophen-2-yl)-5,6-difluoro-2-(2-hexyldecyl)-7-(5-methylthiophen-2-yl)-2*H*-benzo[*d*][1,2,3] triazole] (CD1) and poly[4-(5-(5,10-bis(2-dodecylhexadecyl)-4,4,9,9-tetrafluuoro-7-methyl-4,5,9,10-tetrahydro3a,5,8,10-tetraaza-4,9-diborapyren-2-yl)thiophen-2-yl)-7-(5-methylthiophen-2-yl)benzo[*c*][1,2,5]thiadiazole] (PBN-14) with different M_ns were synthesized in the laboratory according our previous reported method.[50,51]

APSC Devices Fabrication

APSC devices were fabricated with the configuration of ITO/PEDOT:PSS/active layer/LiF/Al. ITO glass substrates were cleaned by sequential ultrasonication in detergent, deionized water, acetone, and isopropyl alcohol, followed by drying at 120 °C for 30 min and treating with UV-ozone for 25 min. Then the PEDOT:PSS solution (Clevios VP AI 4083 from H. C. Starck Inc.) was spin-coated on the ITO glass substrates at 5000 r/min for 40 s to give a thickness of 40 nm, and baked at 120 °C for 30 min. The PEDOT:PSS substrates were transferred to a nitrogen-filled glove box. CD1 and PBN-14 with a weight ratio of 1.5:1 were dissolved together in chlorobenzene (CB) with a total concentration of 10 mg/mL. The solution was stirred at 90 °C for 6 h and not cooling, and then the active layer was hot spin coating. The films thickness was maintained in the range of 80–100 nm. The active layers were annealed at 100 °C for 10 min, after that, 0.5 nm LiF and 100 nm Al were thermally deposited onto the active layer through a shadow mask in a vacuum chamber with a base pressure of 2×10^{-4} Pa. The effective area of the device was defined to be 0.08 cm^2, which was further confined as 0.02 cm^2 by a non-refractive mask to improve the accuracy of measurements.

Hole- and Electron-only Devices Fabrication and Mobility Measurements

The hole and electron mobilities were measured by SCLC method. The hole-only device structure is ITO/PEDOT:PSS (40 nm)/active layer/MoO_3 (10 nm)/Al (100 nm) and the electron-only device structure is ITO/PEIE (10 nm)/active layer/Ca (20 nm)/Al (100 nm), respectively. *J-V* plots in the range of 0–10 V were measured using a Keithley 2400 source meter, and the mobility was obtained by fitting the *J-V* plot near quadratic region according to the modified Mott-Gurney equation:

$$J = (9/8)\,\varepsilon_0\varepsilon_r\mu V^2/d^3 \qquad (1)$$

where J is the current density, ε_0 is permittivity of free space, ε_r is the relative permittivity (assumed to be 3), μ is the zero-field mobility, V is the potential across the device ($V = V_{\text{applied}} - V_{\text{bi}} - V_{\text{series}}$), d is the thickness of active layer. The series and contact resistance of the device (10–20 Ω) were measured using blank device of ITO/PEDOT:PSS/MoO_3/Al or ITO/PEIE/Ca/Al.

Characterization

The *J-V* plots of the APSC devices were measured using a Keithley 2400 source meter under 100 mW/cm^2 AM 1.5G simulated solar light illumination provided by a XES-40S2-CE Class Solar Simulator (Japan, SAN-EI Electric Co., Ltd.). An aperture with an area of 2 mm^2 was used to accurately measure the device performance. The EQE spectra were measured using a Solar Cell Spectral Response Measurement System QE-R3011 (Enlitech Co., Ltd.) under the short-circuit condition at a chopping frequency of 165 Hz. Temperature-dependent UV-Vis absorption spectra of different M_n CD1 and PBN-14 in solution were measured with a Perkin-Elmer Lambda 35 UV-Vis spectrometer. The solution samples were prepared using chlorobenzene solvent with a concentration of 0.1 mg/mL. The transmission electron microscopy (TEM) measurement was performed on a JEOL JEM-1400 transmission electron microscope operating at 120 kV. The atomic force microscopy (AFM) characterization was performed on a SPA 300HV instrument with a SPI 3800 controller (Seiko Instruments). A silicon micro cantilever (spring constant 2 N/m and resonance frequency *ca*. 300 kHz, Olympus Co., Japan) with an etched conical tip was used for the scan. The thickness of films was measured with a XP-plus Stylus Profilometer. Two-dimensional grazing-incidence wide angle X-ray scattering (2D-GIWAXS) was measured at Shanghai Synchrotron Radiation Facility (SSRF) on beam line BL14B1 (λ=0. 124 nm) with a MarCCD area detector at incidence angle of 0.16°. Samples were prepared on Si substrates using identical blend solutions as those used in devices.

RESULTS AND DISCUSSION

As shown in Fig. 1, we select CD1 as the polymer donor and PBN-14 as the polymer acceptor. The opto-electronic properties of CD1 and PBN-14 have been previously reported by us.[50,51] Both CD1 and PBN-14 are semi-crystalline in thin film.

In this work, we synthesized CD1 and PBN-14 with various

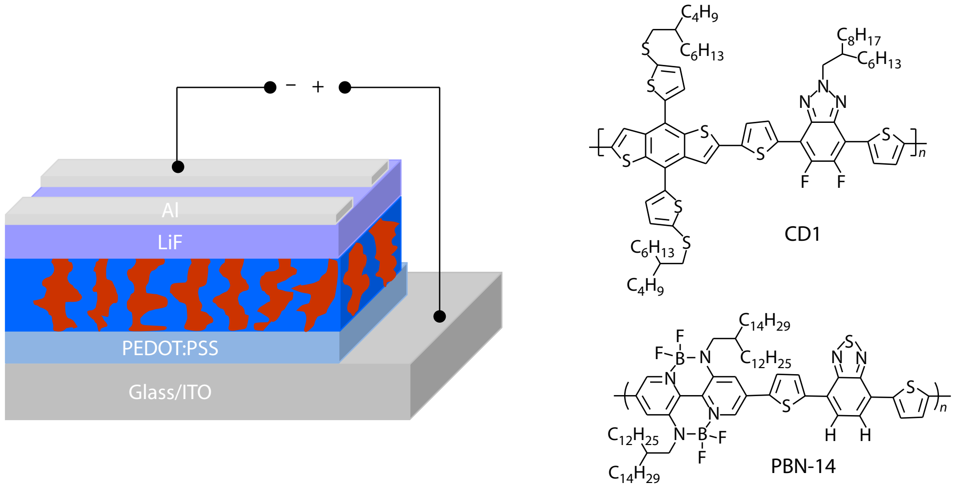

Batch	M_n (kg/mol)	PDI
14C	14.0	2.52
36C	35.5	2.66
56C	56.1	2.82

Batch	M_n (kg/mol)	PDI
33P	32.7	1.92
72P	72.4	1.76
103P	103.4	1.84

Fig. 1 Device architecture of the APSCs, chemical structures and M_ns of CD1 and PBN-14.

M_ns by controlling the polymerization time. We obtained CD1 with the M_n of 14.0, 35.5 and 56.1 kg/mol, which were named as 14C, 36C and 56C respectively. Three batches of PBN-14 with the M_ns of 32.7, 72.4 and 103.4 kg/mol were also synthesized and named as 33P, 72P and 103P, respectively. The polydispersity index (PDI) of CD1 and PBN-14 of various batches is similar (see Fig. 1).

Aggregation tendencies of polymer donors and polymer acceptors in solution greatly affect blend morphology of active layers in APSCs.[52,53] The aggregation tendency was studied by the UV-Vis absorption spectra of the polymers in solution. Figs. 2(a) and 2(b) show the UV-Vis spectra of CD1 and PBN-14 with different M_ns in chlorobenzene solution, respectively. In the absorption spectra of CD1, the ratio of the two absorption peaks can be used to estimate the aggregation tendency of the polymer chains in solution. With the increase of M_n, the relative intensity of the long-wavelength peak at 584 nm increases, indicating stronger aggregation tendency of CD1 polymer chains in chlorobenzene solution. Similar trend is also observed in the absorption spectra of PBN-14 with different M_ns. The increased M_n of PBN-14 also leads to stronger aggregation tendency of PBN-14 polymer chains in solution. The strong aggregation tendency in solution at high M_n is expected to lead to excellent phase separation morphology of active layers of APSCs.

Two-dimensional grazing incidence wide-angle X-ray scattering (2D-GIWAXS) was utilized to characterize the packing of polymer chains of CD1 and PBN-14 in thin film. The 2D-GIWAXS patterns of the polymer films are shown in Fig. 3 and the corresponding data of the GIWAXS patterns are summarized in Table S3 (in the electronic supplementary information, ESI). All the six CD1 and PBN-14 films exhibit the (100) peak mainly in the in-plane direction and the (010) peak in the out-of-plane direction, indicating face-on orientation of the polymer chains in thin film. The M_ns of CD1 and PBN-14 do not affect the orientation of the polymer chains in thin film. We estimate the average crystallization size of the films by calculating the coherence length (CL) of the (100) reflection peak in the in-plane direction and the (010) reflection peak in the out-of-plane direction using the Scherrer equation. The CL values of the (100) peaks of 14C are obviously larger than those of 36C and 56C. The CL values of the (100) peaks of 33P are also larger than those of 72P and 103P. These results probably suggest that high M_n leads to suppressed crystallinity in thin film.

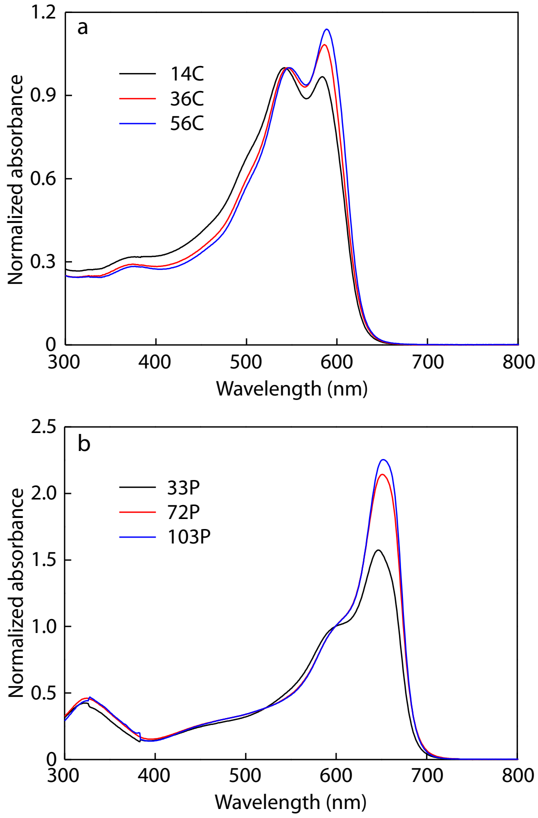

Fig. 2 UV-Vis absorption spectra of (a) CD1 and (b) PBN-14 of different M_ns in chlorobenzene solutions. (The curves from bottom to top: 14C, 36C, 56C in (a) and 33P, 72P, 103P in (b).)

We measured the hole mobility (μ_h) of the three CD1 samples and the electron mobility (μ_e) of the three PBN-14 samples using space charge limited current (SCLC) method with the hole-only devices and the electron-only devices, respectively.[54,55] The current denstiy-voltage (*J-V*) curves of the

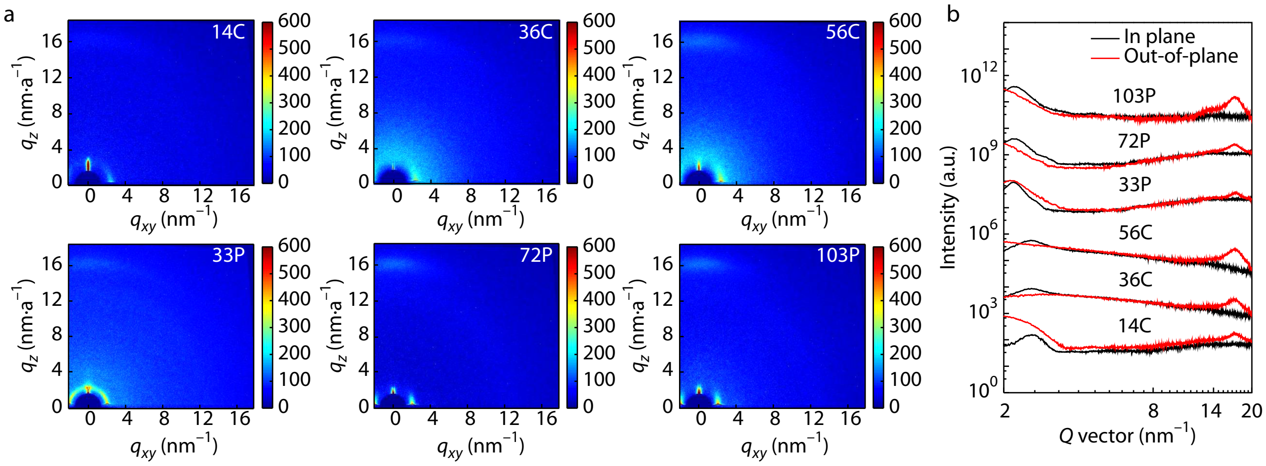

Fig. 3 (a) 2D-GIWAXS patterns and (b) the corresponding in-plane and out-of-plane lines of the films for CD1 and PBN-14 with different M_ns. (The online version is colorful.)

devices are shown in Fig. S4 (in ESI). The μ_h and μ_e values are listed in Table S1 (in ESI). With the increasing M_n, the μ_h of CD1 gradually increases, the μ_e of PBN-14 increases first and then decreases. The three CD1 samples of different M_ns show similar absorption spectra in thin film and similar LUMO/HOMO energy levels. Similar trend is also observed for the three PBN-14 samples. These results indicate that the M_ns of the polymers do not affect the energy levels but affect the charge transporting properties.

APSCs devices with the conventional configuration of ITO/PEDOT:PSS/CD1:PBN-14/LiF/Al were fabricated to investigate the effect of molecualr weights on device performance. CD1 and PBN-14 were dissolved together in chlorobenzene (CB) with a weight ratio of 1.5:1 and a total concentration of 10 mg/mL. The active layer was spin-coated with the solution of CD1 and PBN-14 at 90 °C, followed by thermal annealing at 100 °C for 10 min. The *J-V* curves of the APSCs devices fabricated with various M_n combinations are shown in Fig. 4(a) and the detailed parameters are collected in Table 1. The nine devices exhibit similar open circuit voltage (V_{OC}), different short-circuit current density (J_{SC}) and fill factor (FF). The PCE varies greatly from 4.43% to 10.06%, indicating that M_n of the polymer donors and polymer acceptors play an important role in the APSC device performance. The nearly unaffected V_{OC} is attributed to the little effect of M_n on LUMO/HOMO energy levels of the polymers. The different J_{SC} and FF values are due to the phase separation morphology of the active layers. Fig. 4(b) shows the external quantum efficiency (EQE) curves of the device. The EQE spectra are in accordance with the dependence of the integrated J_{SC} value on different M_n donor-acceptor combinations.

By comparing the PCE of the nine APSCs devices, we analyze the interplay of the M_n of CD1 and PBN-14 on their effect on the device performance. No matter what the M_n of the

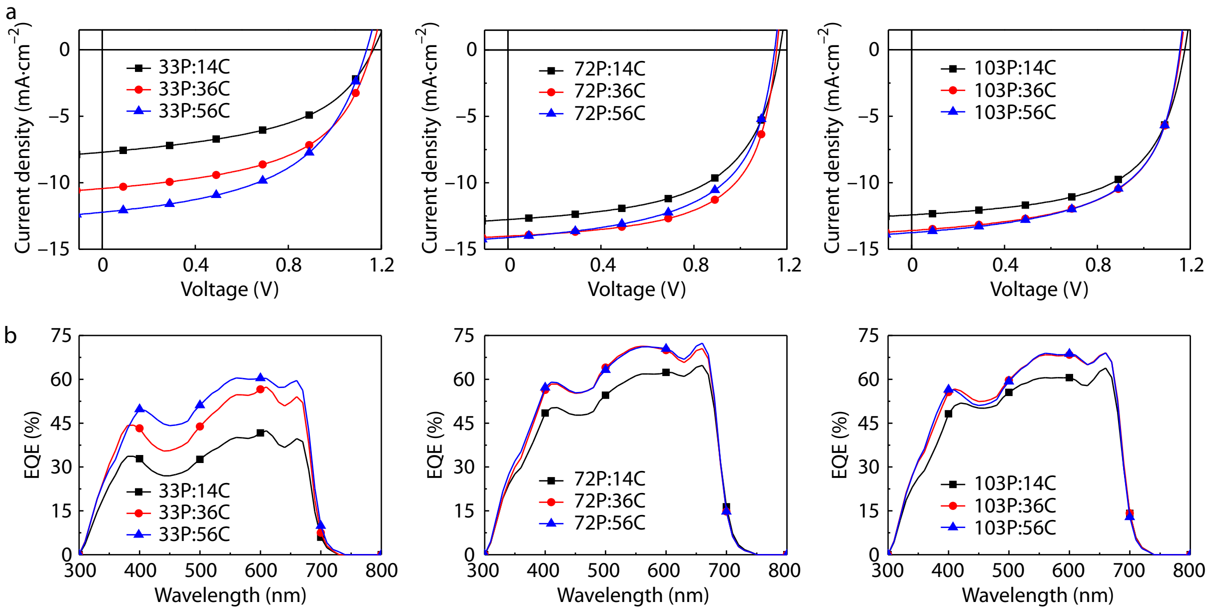

Fig. 4 (a) The *J-V* plots and (b) the EQE spectra of the CD1:PBN-14-based APSCs devices with various M_ns.

Table 1 Photovoltaic parameters of the CD1:PBN-14-based APSCs devices with various M_ns.

Acceptor	Donor	V_{OC} (V)	J_{SC} (mA·cm^{-2})	Cal. J_{SC} (mA·cm^{-2})	FF (%)	PCE [a] (%)
33P	14C	1.17 (1.17±0.01)	7.72 (7.45±0.26)	7.40	49.1 (48.0±1.1)	4.43 (4.05±0.33)
	36C	1.16 (1.16±0.01)	10.44 (10.23±0.20)	10.12	53.0 (52.2±0.8)	6.42 (6.21±0.19)
	56C	1.14 (1.14±0.01)	12.22 (11.91±0.30)	11.96	51.0 (50.0±1.0)	7.10 (6.75±0.34)
72P	14C	1.17 (1.17±0.01)	12.77 (12.50±0.25)	12.43	57.5 (56.1±1.4)	8.59 (8.18±0.41)
	36C	1.16 (1.16±0.01)	14.03 (13.64±0.38)	13.75	61.8 (60.5±1.3)	10.06 (9.69±0.37)
	56C	1.15 (1.15±0.01)	14.12 (13.76±0.35)	13.83	57.8 (57.1±0.7)	9.39 (9.02±0.23)
103P	14C	1.18 (1.18±0.01)	12.42 (12.11±0.31)	12.17	59.4 (58.2±1.2)	8.70 (8.41±0.28)
	36C	1.16 (1.16±0.01)	13.59 (13.35±0.24)	13.34	59.1 (58.4±0.7)	9.32 (9.04±0.25)
	56C	1.16 (1.16±0.01)	13.76 (13.57±0.18)	13.42	58.2 (57.4±0.8)	9.29 (9.01±0.27)

[a] The average parameters were calculated from 10 devices.

polymer acceptor is, the PCEs of the devices of 14C are always lower than those of the corresponding devices of 36C and 56C. Moreover, no matter what M_n of the polymer donor is, the PCEs of the devices of 33P are lower than those of 72P and 103P. According to these results, we believe that sufficiently high M_n of both polymer donor and polymer acceptor are necessary to obtain optimal APSC device peformance. With 33P as the polymer acceptor, the PCE of the devices increases greatly from 4.43% to 7.10% when the M_n of polymer donors increases from 14C to 56C. In comparison, with 72P or 103P as the polymer acceptor, the PCE of the devices are only weakly dependent on the M_n of the polymer donors. The higher M_n of the polymer accptor, the weaker dependence of PCE on the M_n of the polymer donors. Among the nine devices, the highest PCE of 10.06% is obtained with the 72P:36C blend, indicating that medium M_n of both the polymer donor and the polymer acceptor are required for the optimal APSC device performance.

To elucidate the reason behind the effect of M_n on photovoltaic performance, we studied the active layer morphology of the APSCs devices by 2D-GIWAXS, atomic force microscopy (AFM) and transmissions electron microscopy (TEM). The 2D-GIWAXS patterns of the active layers are shown in Fig. 5 and the corresponding data are summarized in Table 2. All the active layers exhibit the (100) diffraction peak at *ca.* 0.24 Å^{-1} and the (010) diffraction peak at 1.70 Å^{-1}. Both the (100) peak and the (010) peak are arributed to the sum of the polymer donor and the polymer acceptor. The (100) peak in the in-plane direction and the (010) peak in the out-of-plane direction suggest that the polymer donor and the polymer acceptor both adopt face-on orientation in the active layers. The M_n does not affect the face-on/edge-on orientation of the polymer donor and the polymer acceptor. As the M_n of CD1 increases, the CL values of the (100) peak and the (010) peak gradually decrease, suggesting decreasing crystallinity of the polymers in the blend films. This trend exists for the donor/

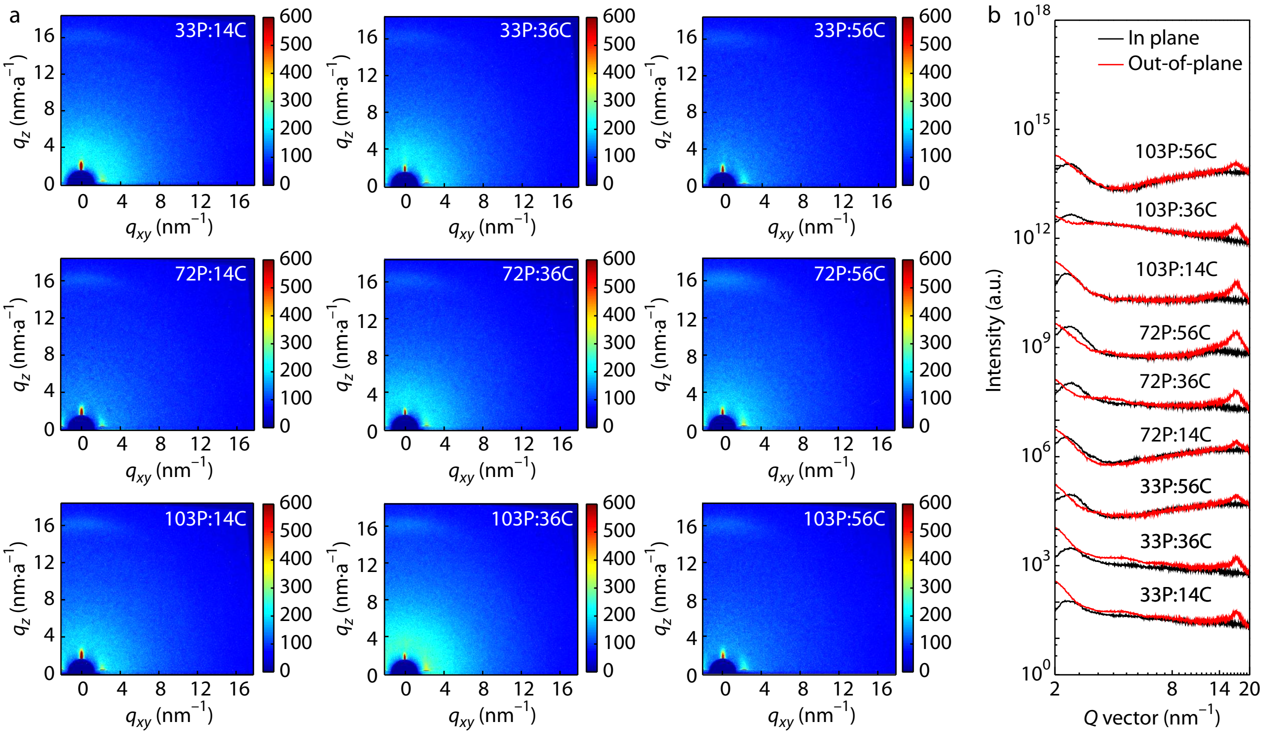

Fig. 5 (a) The 2D-GIWAXS patterns of CD1:PBN-14 active layers with the two polymers of different M_ns; (b) The in-plane and out-of-plane lines of the 2D-GIWAXS patterns. (The online version is colorful.)

Table 2 Characteristics of the (100) peak in the in-plane direction and the (010) peak in the out-of-plane direction of the 2D-GIWAXS patterns for CD1:PBN-14 active layers with the two polymers for different M_ns.

Film	100 (In-plane direction)				010 (Out-of-plane direction)			
	Location (Å^{-1})	*d*-Spacing (Å)	FWHM (Å^{-1})	CL (Å)	Location (Å^{-1})	*d*-Spacing (Å)	FWHM (Å^{-1})	CL (Å)
33P:14C	0.24	25.75	0.069	82	1.70	3.69	0.171	33
33P:36C	0.25	25.54	0.071	77	1.70	3.69	0.186	30
33P:56C	0.23	26.97	0.090	63	1.70	3.69	0.219	26
72P:14C	0.23	27.56	0.066	86	1.71	3.68	0.187	30
72P:36C	0.24	25.75	0.069	82	1.70	3.69	0.195	29
72P:56C	0.24	26.29	0.072	79	1.70	3.69	0.227	25
103P:14C	0.24	26.62	0.059	96	1.70	3.69	0.177	32
103P:14C	0.24	25.96	0.078	72	1.70	3.69	0.184	31
103P:36C	0.24	26.51	0.083	68	1.70	3.69	0.226	25

acceptor combinations with all the three polymer acceptors. For the dependence of CL values on the M_n of polymer acceptors, no clear correlation can be observed. Among the nine active layers, the one of 72P:36C blend with the best photovoltaic performance shows medium CL values of both the (100) peak and the (010) peak.

Fig. 6 shows the AFM height images of the various CD1:PBN-14 combinations. Except those of the 33P:14C blend and the 33P:36C blend, the surfaces of the other seven active layers all show bicontinuous fiberous network microstructure. The fiberous microstructure are beneficial for exciton diffusion, exciton dissociation and charge transporting.[56–59] The AFM height image results are consistent with the poor photovoltaic performance of the 33P:14C and 33P:36C blends as well as the excellent photovoltaic performance of the other seven active layers. The higher M_n of either the polymer donor or the polymer acceptor, the more surface microstructures with thin, long and bicontinuous morphologies. This result indicates that high M_n is dominant for the bicontinuous fiberous network microstructure of the active layer of APSCs. The root-mean-square roughness (R_q) values of the AFM images are also shown in Fig. 6. Obviously, with the in-

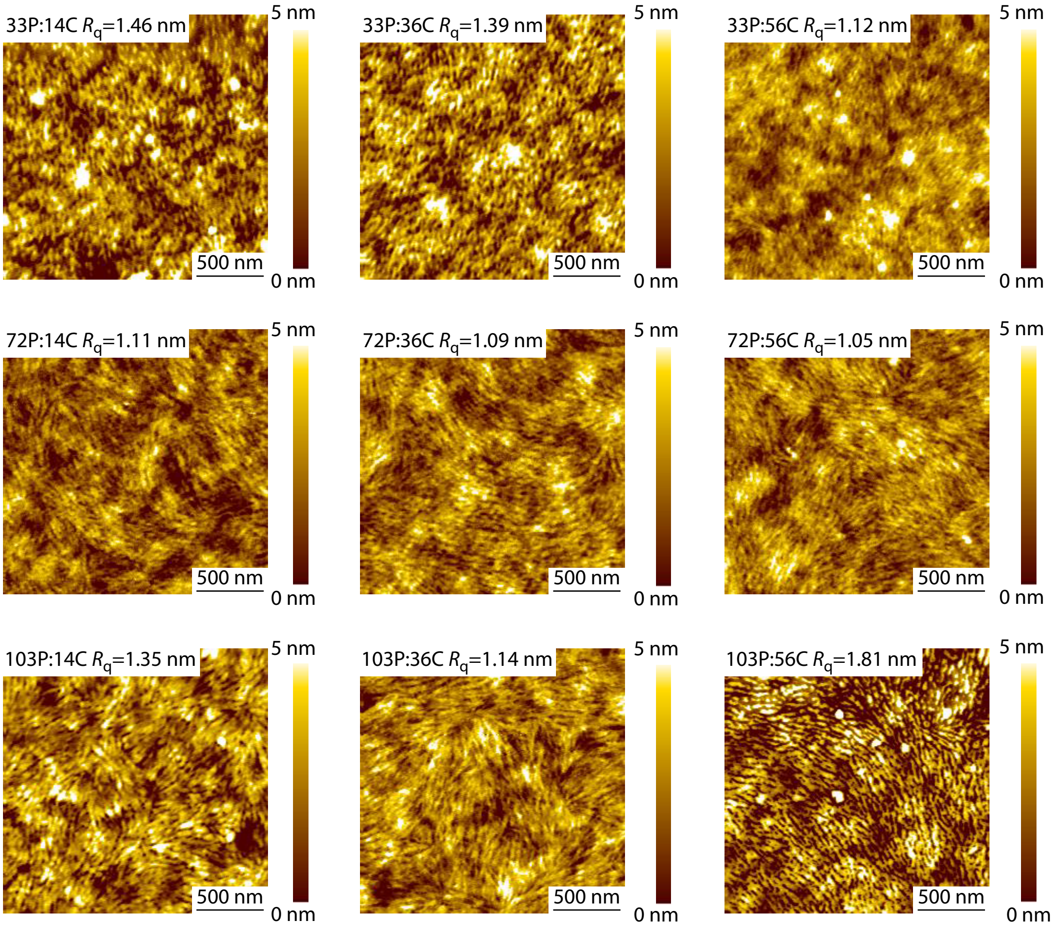

Fig. 6 AFM height images of CD1:PBN-14 active layers with the two polymers of different M_ns.

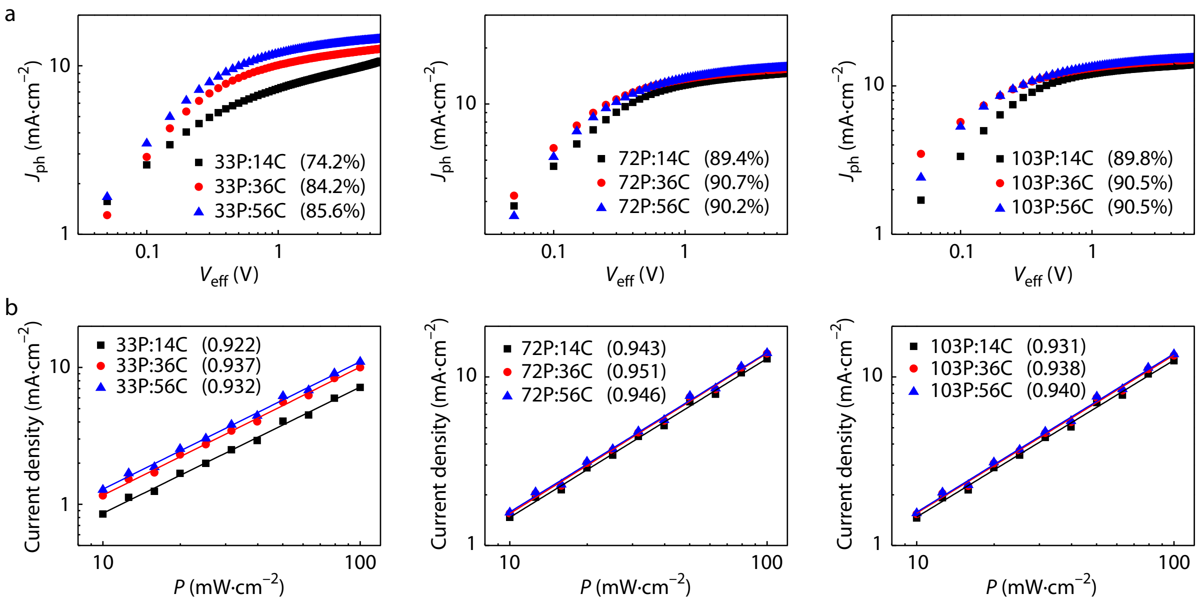

Fig. 7 (a) J_{ph}-V_{eff} plots and (b) light-intensity-dependent J_{SC} of the APSC devices.

creasing M_n of the polymer donor, the R_q values decreases. An exception is the 103P:56C blend, which exhibits rough surface with large R_q value of 1.86 nm. When the M_n of PBN-14 is 72P, all the three active layers with various M_ns of CD1 show smooth surface with small R_q values.

Based on the above result on active layer morphology, we analyze the effects of M_n on phase separation morphology of polymer donor/polymer acceptor blends. High M_n plays an important role in the formation of bicontinuous fibrous network morphology of active layers of APSCs. When both CD1 and PBN-14 have low M_n, the active layer morphology is poor and the PCE is low. At least one polymer should have high M_n to ensure the bicontinuous fibrous network morphology. When the M_n of PBN-14 is high, the resulting active layers all exhibit bicontinuous fibrous network morphology and the PCE of the APSC devices is insensitive to the M_n of CD1. Probably, the aggregation and crystallization of PBN-14 play a more important role in the phase separation of the active layers than those of CD1. This maybe is due to the stronger aggregation tendency in solution and the higher M_n on-general of PBN-14 than those of CD1.

To understand the reason for the difference of the APSC device performance, we studied the charge transport, collection, and recombination behaviors of the devices. The hole and electron mobilities of the devices were estimated by SCLC method with the *J*-*V* plots in dark of the hole-only and the electron-only devices. Fig. S5 (in ESI) shows the *J*-*V* curves and Table S2 (in ESI) lists the hole and electron mobilities. Irrespective of the M_n of PBN-14, as the M_n of CD1 increases, the μ_h of the blend films gradually increases. However, the dependence of μ_e of the blend films on the M_n of CD1 is different at various M_ns of PBN-14. This is attributed to the improved formation of continueous networks of CD1 phase in the blend films at high M_n. The formation of continueous networks of CD1 phase also affects the networks of PBN-14 phase. To study the exciton dissociation and charge collection probabilities of the APSC devices, we measured the dependence of photocurrent density (J_{ph}) on effective voltage (V_{eff}) of the devices. From the J_{ph}-V_{eff} curves as shown in Fig. 7(a), saturated photocurrent density (J_{sat}) and charge collection probabilities (J_{ph}/J_{sat}) can be estimated. When the M_n of the acceptor PBN-14 is high (72P and 103P), all the devices exhibit high charge collection probability of about 90%. When the polymer acceptor is 33P with low M_n, as the M_n of the polymer donor CD1 increases, the J_{ph}/J_{sat} gradually increases, implying increasing charge collection probability. We measured the dependence of J_{SC} on light intensity (I) of the APSC devices to evaluate the bimolecular recombination behaviors. The results are shown in Fig. 7(b). The relationship between J_{SC} and I is defined as $J_{SC} \propto I^{\alpha}$, where α is the power-law exponent. The α value close to 1 represents weak bimolecular recombination in the device.[60,61] The α values of all the nine APSC devices are in the range of 0.922–0.951. This result suggests that all the devices have the moderate degree of bimolecular recombination. Among the nine APSC devices, the device based on 72P:36C blend exhibits the highest charge collection probability and the weakest bimolecular recombination, which is in accordance with the best photovoltaic performance.

CONCLUSIONS

In summary, we systematically study the effects of M_n of the two polymers on active layer morphology and photovoltaic performance of APSCs by synthesizing a series of different M_n polymer donor CD1 and polymer acceptor PBN-14. The active layers of CD1:PBN-14 blends exhibit bicontinuous fibrous network morphololgy and achieve PCE of 10% in APSC devices. To get the desired active layer morphology of polymer donor/polymer acceptor blends, at least one polymer should have high M_n. When M_n of the polymer acceptor is high, the APSC device performance is insensitive to the M_n of the polymer donor. The optimal APSC device performance is obtained when the M_n of both the polymer donor and the polymer acceptor are medium. These results provide a comprehensive and deep understanding of the matching of M_n of polymer donors and polymer acceptors in high-performance APSCs.

Electronic Supplementary Information

Electronic supplementary information (ESI) is available free of charge in the online version of this article at http://doi.org/10.1007/s10118-021-2609-9.

ACKNOWLEDGMENTS

This work was financially supported by the National Key Research and Development Program of China (Nos. 2018YFE0100600 and 2019YFA0705902) funded by the Ministry of Science and Technology and the National Natural Science Foundation of China (Nos. 21625403 and 21875244). The authors also thank the Shanghai Synchrotron Radiation Facility (SSRF) for help with 2D-GIWAXS measurements.

REFERENCES

1 Yu, G.; Gao, J.; Hummelen, J. C.; Wudl, F.; Heeger, A. J. Polymer photovoltaic cells: enhanced efficiencies *via* a network of internal donor-acceptor heterojunctions. *Science* **1995**, *270*, 1789−1791.

2 Zhang, G.; Zhao, J.; Chow, P. C. Y.; Jiang, K.; Zhang, J.; Zhu, Z.; Zhang, J.; Huang, F.; Yan, H. Nonfullerene acceptor molecules for bulk heterojunction organic solar cells. *Chem. Rev.* **2018**, *118*, 3447−3507.

3 Hou, J.; Inganas, O.; Friend, R. H.; Gao, F. Organic solar cells based on non-fullerene acceptors. *Nat. Mater.* **2018**, *17*, 119−128.

4 Yan, C.; Barlow, S.; Wang, Z.; Yan, H.; Jen, A. K. Y.; Marder, S. R.; Zhan, X. Non-fullerene acceptors for organic solar cells. *Nat. Rev. Mater.* **2018**, *3*, 18003.

5 Cheng, P.; Li, G.; Zhan, X.; Yang, Y. Next-generation organic photovoltaics based on non-fullerene acceptors. *Nat. Photonics* **2018**, *12*, 131−142.

6 Cui, Y.; Wang, Y.; Bergqvist, J.; Yao, H.; Xu, Y.; Gao, B.; Yang, C.; Zhang, S.; Inganäs, O.; Gao, F.; Hou, J. Wide-gap non-fullerene acceptor enabling high-performance organic photovoltaic cells for indoor applications. *Nature Energy* **2019**, *4*, 768−775.

7 Wu, Q.; Guo, J.; Sun, R.; Guo, J.; Jia, S.; Li, Y.; Wang, J.; Min, J. Slot-die printed non-fullerene organic solar cells with the highest efficiency of 12.9% for low-cost PV-driven water splitting. *Nano Energy* **2019**, *61*, 559−566.

8 Lee, C.; Lee, S.; Kim, G. U.; Lee, W.; Kim, B. J. Recent advances, design guidelines, and prospects of all-polymer solar cells. *Chem. Rev.* **2019**, *119*, 8028−8086.

9 Guo, Y.; Li, Y.; Awartani, O.; Han, H.; Zhao, J.; Ade, H.; Yan, H.; Zhao, D. Improved performance of all-polymer solar cells enabled by naphthodiperylenetetraimide-based polymer acceptor. *Adv. Mater.* **2017**, *29*, 1700309.

10 Guo, Y.; Li, Y.; Awartani, O.; Zhao, J.; Han, H.; Ade, H.; Zhao, D.; Yan, H. A vinylene-bridged perylenediimide-based polymeric acceptor enabling efficient all-polymer solar cells processed under ambient conditions. *Adv. Mater.* **2016**, *28*, 8483−8489.

11 Yang, J.; Xiao, B.; Tang, A.; Li, J.; Wang, X.; Zhou, E. Aromatic-diimide-based n-type conjugated polymers for all-polymer solar cell applications. *Adv. Mater.* **2019**, *31*, e1804699.

12 Yang, J.; Yin, Y.; Chen, F.; Zhang, Y.; Xiao, B.; Zhao, L.; Zhou, E. Comparison of three n-type copolymers based on benzodithiophene and naphthalene diimide/perylene diimide/fused perylene diimides for all-polymer solar cells application. *ACS Appl. Mater. Interfaces* **2018**, *10*, 23263−23269.

13 Zhang, Q.; Chen, Z.; Ma, W.; Xie, Z.; Han, Y. Optimizing domain size and phase purity in all-polymer solar cells by solution ordered aggregation and confinement effect of the acceptor. *J. Mater. Chem. C* **2019**, *7*, 12560−12571.

14 Wang, Y.; Zhu, Q.; Naveed, H. B.; Zhao, H.; Zhou, K.; Ma, W. Sequential blade-coated acceptor and donor enables simultaneous enhancement of efficiency, stability, and mechanical properties for organic solar cells. *Adv. Energy Mater.* **2020**, *10*, 1903609.

15 Dou, C. D.; Ding, Z. C.; Zhang, Z. J.; Xie, Z. Y.; Liu, J.; Wang, L. X. Developing conjugated polymers with high electron affinity by replacing a C-C Unit with a B←N unit. *Angew. Chem. Int. Ed.* **2015**, *54*, 3648−3652.

16 Zhao, R.; Dou, C.; Xie, Z.; Liu, J.; Wang, L. Polymer acceptor based on B←N units with enhanced electron mobility for efficient all-polymer solar cells. *Angew. Chem. Int. Ed.* **2016**, *55*, 5313−5317.

17 Zhao, R.; Dou, C.; Liu, J.; Wang, L. An alternating polymer of two building blocks based on B←N unit: non-fullerene acceptor for organic photovoltaics. *Chinese J. Polym. Sci.* **2016**, *35*, 198−206.

18 Dou, C.; Liu, J.; Wang, L. Conjugated polymers containing B←N unit as electron acceptors for all-polymer solar cells. *Sci. China Chem.* **2017**, *60*, 450−459.

19 Shi, S.; Chen, P.; Chen, Y.; Feng, K.; Liu, B.; Chen, J.; Liao, Q.; Tu, B.; Luo, J.; Su, M.; Guo, H.; Kim, M. G.; Facchetti, A.; Guo, X. A Narrow-bandgap n-type polymer semiconductor enabling efficient all-polymer solar cells. *Adv. Mater.* **2019**, *31*, e1905161.

20 Sun, H.; Tang, Y.; Koh, C. W.; Ling, S.; Wang, R.; Yang, K.; Yu, J.; Shi, Y.; Wang, Y.; Woo, H. Y.; Guo, X. High-performance all-polymer solar cells enabled by an n-type polymer based on a fluorinated imide-functionalized arene. *Adv. Mater.* **2019**, *31*, e1807220.

21 Lin, B.; Zhang, L.; Zhao, H.; Xu, X.; Zhou, K.; Zhang, S.; Gou, L.; Fan, B.; Zhang, L.; Yan, H.; Gu, X.; Ying, L.; Huang, F.; Cao, Y.; Ma, W. Molecular packing control enables excellent performance and mechanical property of blade-cast all-polymer solar cells. *Nano Energy* **2019**, *59*, 277−284.

22 Kim, W.; Choi, J.; Kim, J. H.; Kim, T.; Lee, C.; Lee, S.; Kim, M.; Kim, B. J.; Kim, T. S. Comparative study of the mechanical properties of all-polymer and fullerene–polymer solar cells: the importance of polymer acceptors for high fracture resistance. *Chem. Mater.* **2018**, *30*, 2102−2111.

23 Zhang, Y.; Xu, Y.; Ford, M. J.; Li, F.; Sun, J.; Ling, X.; Wang, Y.; Gu, J.; Yuan, J.; Ma, W. Thermally stable all-polymer solar cells with high tolerance on blend ratios. *Adv. Energy Mater.* **2018**, *8*, 1800029.

24 Lee, W.; Kim, J. H.; Kim, T.; Kim, S.; Lee, C.; Kim, J. S.; Ahn, H.; Kim, T. S.; Kim, B. J. Mechanically robust and high-performance ternary solar cells combining the merits of all-polymer and fullerene blends. *J. Mater. Chem. A* **2018**, *6*, 4494−4503.

25 Kang, H.; Lee, W.; Oh, J.; Kim, T.; Lee, C.; Kim, B. J. From fullerene-polymer to all-polymer solar cells: the importance of molecular packing, orientation, and morphology control. *Acc. Chem. Res.* **2016**, *49*, 2424−2434.

26 Wang, W.; Wu, Q.; Sun, R.; Guo, J.; Wu, Y.; Shi, M.; Yang, W.; Li, H.; Min, J. Controlling molecular mass of low-band-gap polymer

acceptors for high-performance all-polymer solar cells. *Joule* **2020**, *4*, 1070−1086.

27 Yang, H.; Fan, H.; Wang, Z.; Yan, H.; Dong, Y.; Cui, C.; Ade, H.; Li, Y. Impact of isomer design on physicochemical properties and performance in high-efficiency all-polymer solar cells. *Macromolecules* **2020**, *53*, 9026−9033.

28 Sun, H.; Yu, H.; Shi, Y.; Yu, J.; Peng, Z.; Zhang, X.; Liu, B.; Wang, J.; Singh, R.; Lee, J.; Li, Y.; Wei, Z.; Liao, Q.; Kan, Z.; Ye, L.; Yan, H.; Gao, F.; Guo, X. A narrow-bandgap n-type polymer with an acceptor-acceptor backbone enabling efficient all-polymer solar cells. *Adv. Mater.* **2020**, *32*, e2004183.

29 Yu, H.; Qi, Z.; Yu, J.; Xiao, Y.; Sun, R.; Luo, Z.; Cheung, A. M. H.; Zhang, J.; Sun, H.; Zhou, W.; Chen, S.; Guo, X.; Lu, X.; Gao, F.; Min, J.; Yan, H. Fluorinated end group enables high-performance all-polymer solar cells with near-infrared absorption and enhanced device efficiency over 14%. *Adv. Energy Mater.* **2020**, *11*, 2003171.

30 Zhu, C.; Li, Z.; Zhong, W.; Peng, F.; Zeng, Z.; Ying, L.; Huang, F.; Cao, Y. Constructing a new polymer acceptor enabled non-halogenated solvent-processed all-polymer solar cell with an efficiency of 13.8%. *Chem. Commun.* **2021**, *57*, 935−938.

31 Fan, Q.; An, Q.; Lin, Y.; Xia, Y.; Li, Q.; Zhang, M.; Su, W.; Peng, W.; Zhang, C.; Liu, F.; Hou, L.; Zhu, W.; Yu, D.; Xiao, M.; Moons, E.; Zhang, F.; Anthopoulos, T. D.; Inganäs, O.; Wang, E. Over 14% efficiency all-polymer solar cells enabled by a low bandgap polymer acceptor with low energy loss and efficient charge separation. *Energy Environ. Sci.* **2020**, *13*, 5017−5027.

32 Fu, H.; Li, Y.; Yu, J.; Wu, Z.; Fan, Q.; Lin, F.; Woo, H. Y.; Gao, F.; Zhu, Z.; Jen, A. K. High efficiency (15.8%) all-polymer solar cells enabled by a regioregular narrow bandgap polymer acceptor. *J. Am. Chem. Soc* **2021**, *143*, 2665−2670.

33 Luo, Z.; Liu, T.; Ma, R.; Xiao, Y.; Zhan, L.; Zhang, G.; Sun, H.; Ni, F.; Chai, G.; Wang, J.; Zhong, C.; Zou, Y.; Guo, X.; Lu, X.; Chen, H.; Yan, H.; Yang, C. Precisely controlling the position of bromine on the end group enables well-regular polymer acceptors for all-polymer solar cells with efficiencies over 15%. *Adv. Mater.* **2020**, *32*, e2005942.

34 Peng, F.; An, K.; Zhong, W.; Li, Z.; Ying, L.; Li, N.; Huang, Z.; Zhu, C.; Fan, B.; Huang, F.; Cao, Y. A universal fluorinated polymer acceptor enables all-polymer solar cells with >15% efficiency. *ACS Energy Lett.* **2020**, *5*, 3702−3707.

35 Zhang, L.; Jia, T.; Pan, L.; Wu, B.; Wang, Z.; Gao, K.; Liu, F.; Duan, C.; Huang, F.; Cao, Y. 15.4% Efficiency all-polymer solar cells. *Sci. China Chem.* **2021**, *64*, 408–412.

36 Wadsworth, A.; Hamid, Z.; Bidwell, M.; Ashraf, R. S.; Khan, J. I.; Anjum, D. H.; Cendra, C.; Yan, J.; Rezasoltani, E.; Guilbert, A. A. Y.; Azzouzi, M.; Gasparini, N.; Bannock, J. H.; Baran, D.; Wu, H.; de Mello, J. C.; Brabec, C. J.; Salleo, A.; Nelson, J.; Laquai, F.; McCulloch, I. Progress in poly (3-hexylthiophene) organic solar cells and the influence of its molecular weight on device performance. *Adv. Energy Mater.* **2018**, *8*, 1801001.

37 Zhang, Y.; Xu, X.; Lu, J.; Zhang, S. Effect of polymer molecular weight on J51 based organic solar cells. *RSC Adv.* **2019**, *9*, 14657−14661.

38 Zhang, Z.; Wang, T.; Ding, Z.; Miao, J.; Wang, J.; Dou, C.; Meng, B.; Liu, J.; Wang, L. Small molecular donor/polymer acceptor type organic solar cells: effect of molecular weight on active layer morphology. *Macromolecules* **2019**, *52*, 8682−8689.

39 Wu, Y.; Schneider, S.; Walter, C.; Chowdhury, A. H.; Bahrami, B.; Wu, H. C.; Qiao, Q.; Toney, M. F.; Bao, Z. Fine-tuning semiconducting polymer self-aggregation and crystallinity enables optimal morphology and high-performance printed all-polymer solar cells. *J. Am. Chem. Soc.* **2020**, *142*, 392−406.

40 Park, J. S.; Choi, N.; Lee, C.; Lee, S.; Ha, J. W.; Hwang, D. H.; Kim, B. J. Elucidating roles of polymer donor aggregation in all-polymer and non-fullerene small-molecule-polymer solar cells. *Chem. Mater.* **2020**, *32*, 3585−3596.

41 Fan, B.; Ying, L.; Wang, Z.; He, B.; Jiang, X. F.; Huang, F.; Cao, Y. Optimisation of processing solvent and molecular weight for the production of green-solvent-processed all-polymer solar cells with a power conversion efficiency over 9%. *Energy Environ. Sci.* **2017**, *10*, 1243−1251.

42 Wang, N.; Yu, Y.; Zhao, R.; Ding, Z.; Liu, J.; Wang, L. Improving active layer morphology of all-polymer solar cells by solution temperature. *Macromolecules* **2020**, *53*, 3325−3331.

43 Wang, N.; Long, X.; Ding, Z.; Feng, J.; Lin, B.; Ma, W.; Dou, C.; Liu, J.; Wang, L. Improving active layer morphology of all-polymer solar cells by dissolving the two polymers individually. *Macromolecules* **2019**, *52*, 2402−2410.

44 Chen, S.; An, Y.; Dutta, G. K.; Kim, Y.; Zhang, Z. G.; Li, Y.; Yang, C. A synergetic effect of molecular weight and fluorine in all-polymer solar cells with enhanced performance. *Adv. Funct. Mater.* **2017**, *27*, 1603564.

45 Kang, H.; Uddin, M. A.; Lee, C.; Kim, K. H.; Nguyen, T. L.; Lee, W.; Li, Y.; Wang, C.; Woo, H. Y.; Kim, B. J. Determining the role of polymer molecular weight for high-performance all-polymer solar cells: its effect on polymer aggregation and phase separation. *J. Am. Chem. Soc.* **2015**, *137*, 2359−2365.

46 Tran, D. K.; Robitaille, A.; Hai, I. J.; Ding, X.; Kuzuhara, D.; Koganezawa, T.; Chiu, Y. C.; Leclerc, M.; Jenekhe, S. A. , Elucidating the impact of molecular weight on morphology, charge transport, photophysics and performance of all-polymer solar cells. *J. Mater. Chem. A* **2020**, *8*, 21070−21083.

47 Li, Z.; Zhong, W.; Ying, L.; Liu, F.; Li, N.; Huang, F.; Cao, Y. Morphology optimization *via* molecular weight tuning of donor polymer enables all-polymer solar cells with simultaneously improved performance and stability. *Nano Energy* **2019**, *64*, 103931.

48 Wang, G.; Eastham, N. D.; Aldrich, T. J.; Ma, B.; Manley, E. F.; Chen, Z.; Chen, L. X.; de la Cruz, M. O.; Chang, R. P. H.; Melkonyan, F. S.; Facchetti, A.; Marks, T. J. Photoactive blend morphology engineering through systematically tuning aggregation in all-polymer solar cells. *Adv. Energy Mater.* **2018**, *8*, 1702173.

49 Zhou, N.; Dudnik, A. S.; Li, T. I.; Manley, E. F.; Aldrich, T. J.; Guo, P.; Liao, H. C.; Chen, Z.; Chen, L. X.; Chang, R. P.; Facchetti, A.; Olvera de la Cruz, M.; Marks, T. J. All-polymer solar cell performance optimized via systematic molecular weight tuning of both donor and acceptor polymers. *J. Am. Chem. Soc.* **2016**, *138*, 1240−1251.

50 Zhao, R.; Wang, N.; Yu, Y.; Liu, J. Organoboron polymer for 10% efficiency all-polymer solar cells. *Chem. Mater.* **2020**, *32*, 1308−1314.

51 Miao, J.; Meng, B.; Ding, Z.; Liu, J.; Wang, L. Organic solar cells based on small molecule donors and polymer acceptors operating at 150 °C. *J. Mater. Chem. A* **2020**, *8*, 10983−10988.

52 Zhao, R.; Lin, B.; Feng, J.; Dou, C.; Ding, Z.; Ma, W.; Liu, J.; Wang, L. Amorphous polymer acceptor containing B ← N units matches various polymer donors for all-polymer solar cells. *Macromolecules* **2019**, *52*, 7081−7088.

53 Du, J.; Hu, K.; Meng, L.; Angunawela, I.; Zhang, J.; Qin, S.; Liebman-Pelaez, A.; Zhu, C.; Zhang, Z.; Ade, H.; Li, Y. High-performance all-polymer solar cells: synthesis of polymer acceptor by a random

ternary copolymerization strategy. *Angew. Chem. Int. Ed.* **2020**, *59*, 15181–15185.

54 Xie, Q.; Liao, X.; Chen, L.; Zhang, M.; Gao, K.; Huang, B.; Xu, H.; Liu, F.; Jen, A. K. Y.; Chen, Y. Random copolymerization realized high efficient polymer solar cells with a record fill factor near 80%. *Nano Energy* **2019**, *61*, 228–235.

55 Yuan, J.; Qiu, L.; Zhang, Z.; Li, Y.; He, Y.; Jiang, L.; Zou, Y. A simple strategy to the side chain functionalization on the quinoxaline unit for efficient polymer solar cells. *Chem. Commun.* **2016**, *52*, 6881–6884.

56 Liu, T.; Huo, L.; Chandrabose, S.; Chen, K.; Han, G.; Qi, F.; Meng, X.; Xie, D.; Ma, W.; Yi, Y.; Hodgkiss, J. M.; Liu, F.; Wang, J.; Yang, C.; Sun, Y. Optimized fibril network morphology by precise side-chain engineering to achieve high-performance bulk-heterojunction organic solar cells. *Adv. Mater.* **2018**, *30*, e1707353.

57 Xia, T.; Cai, Y.; Fu, H.; Sun, Y. Optimal bulk-heterojunction morphology enabled by fibril network strategy for high-performance organic solar cells. *Sci. China Chem.* **2019**, *62*, 662–668.

58 Song, J.; Ye, L.; Li, C.; Xu, J.; Chandrabose, S.; Weng, K.; Cai, Y.; Xie, Y.; O'Reilly, P.; Chen, K.; Zhou, J.; Zhou, Y.; Hodgkiss, J. M.; Liu, F.; Sun, Y. An optimized fibril network morphology enables high-efficiency and ambient-stable polymer solar cells. *Adv. Sci.* **2020**, *7*, 2001986.

59 Xie, Y.; Cai, Y.; Zhu, L.; Xia, R.; Ye, L.; Feng, X.; Yip, H. L.; Liu, F.; Lu, G.; Tan, S.; Sun, Y. Fibril network strategy enables high-performance semitransparent organic solar cells. *Adv. Funct. Mater.* **2020**, *30*, 2002181.

60 Blom, P. W. M.; Mihailetchi, V. D.; Koster, L. J. A.; Markov, D. E. Device physics of polymer:fullerene bulk heterojunction solar cells. *Adv. Mater.* **2007**, *19*, 1551–1566.

61 Li, M.; Zhou, Y.; Zhang, J.; Song, J.; Bo, Z. Tuning the dipole moments of nonfullerene acceptors with an asymmetric terminal strategy for highly efficient organic solar cells. *J. Mater. Chem. A* **2019**, *7*, 8889–8896.